Mode-Expanded 1.55-μm InP–InGaAsP Fabry–Pérot Lasers Using ARROW Waveguides for Efficient Fiber Coupling

Marko Galarza, Kurt De Mesel, Steven Verstuyft, David Fuentes, Cándido Aramburu, Manuel López-Amo, *Senior Member, IEEE*, Ingrid Moerman, *Member, IEEE*, Peter Van Daele, *Member, IEEE*, and Roel G. Baets, *Senior Member, IEEE*

***Abstract*—We report on a new concept for InGaAsP–InP 1.55-μm lasers with integrated spot-size converters based on antiresonant reflecting optical waveguides (ARROWs). The mode expanders consist of a tapered active region on top of a fiber-matched passive vertical ARROW waveguide. The large fundamental leaky mode with its low propagation loss makes ARROW waveguides useful for fiber coupling functions and avoids typical growth-related problems as encountered with traditional designs. The tapers exhibit a low transformation loss and narrowed far-field emission patterns (10.4° × 22°) and reduce the coupling loss to standard single-mode fibers from 8 to 2.6 dB. We also present the design and the results obtained with a relaxed ARROW design with thinner ARROW layers to reduce the overall layer stack thickness considerably, without affecting the fiber-coupling performance. The antiresonant effect has also been used for the lateral confinement of the fiber-matched mode. This feature makes the presented spot-size transformer as simple to fabricate as a standard waveguide, only requiring a planar growth step and a single conventional etch process. The fabricated tapers exhibit a low transformation loss and minimum far-field divergence angles of 13.8° × 30.8°, reducing the coupling loss to a standard single-mode fiber from 8 to 4 dB. We also analyze by simulation two variants of the concept proposed in this work, including a taper structure for a buried waveguide, which are expected to show better performance. Simulation results show fiber-coupling efficiencies as low as 2.4 and 1.1 dB and reduced far-field divergence angles as low as 7.2° × 14° and 7.2° × 9° for both variants.**

***Index Terms*—Optical couplers, optical waveguides, semiconductor device modeling, semiconductor device packaging, semiconductor lasers.**

I. Introduction

THERE exist two rationales for the use of integrated spot-size converters (SSCs) in the development of low-cost optoelectronic devices. One is the pigtailing or fiber attachment of III–V semiconductor photonic integrated circuits (PICs), mostly active devices containing lasers or semiconductor optical amplifiers. The other is the integration of such PICs with silica-on-silicon waveguides for the development of hybrid devices.

The typical refractive index difference Δn in a semiconductor waveguide is generally larger than 1×10^{-1}, leading to mode sizes smaller than 2 μm. Besides, due to the planar technology used in the fabrication of semiconductor waveguides, the mode shape is highly asymmetric. The very small refractive index difference in a single-mode glass fiber or silica waveguide ($\Delta n < 5 \times 10^{-3}$), on the other hand, results in a weakly guided circular mode with a typical mode size of 8–10 μm. Direct butt-coupling between an optoelectronic device and a fiber causes typically 7–10 dB loss.

The function of an integrated SSC is to enlarge and reshape the small and asymmetric mode of the III–V semiconductor waveguide component to a large and circular mode that is better adapted to the fiber or silica waveguide [1]. In this way, it provides high coupling efficiencies and large alignment tolerances that enable the use of passive alignment schemes that drastically reduce the packaging cost. The use of microlenses or tapered/lensed fibers [2] that image one mode onto the other is an alternate solution that also improves the coupling loss, but at the expense of the alignment tolerances, which are then in the submicrometer range.

Over the past ten years, much research has focused on the integration of mode size converters with waveguide components in order to improve the coupling efficiency [3], [4]. Most of these approaches involve complex growth and/or processing steps, requiring extensive process development. Nevertheless, there is one group of devices that is particularly interesting since it only requires a single standard planar epitaxial growth step and conventional lithography and etching processes [5]–[7]. These devices incorporate a large fiber-matched rib waveguide that operates close to cutoff. In InP technology, this involves the growth of quaternary materials exhibiting a slightly higher refractive index than the InP-substrate. These low-refractive indexes are achieved by means of low Ga- and As-fraction quaternary materials, which are difficult to grow. This problem was solved in [8] by introducing a diluted structure.

We have demonstrated an alternative solution in recent work [9], where the thick quaternary layer is replaced by an easy-to-grow InP layer in an antiresonant reflecting optical waveguide (ARROW) configuration [10], [11]. In the tapered 1.55-μm laser presented in [9], a laser rib is laterally tapered

Manuscript received August 30, 2002; revised September 25, 2002. This work was supported in part by Spanish CICYT under Project TIC2001-0877-C02-02 and by Nafarroako Gobernua under a grant.

M. Galarza, K. De Mesel, S. Verstuyft, I. Moerman, P. Van Daele, and R. G. Baets are with the Department of Information Technology, Ghent University-IMEC, B-9000 Ghent, Belgium (e-mail: mgalarza@intec.rug.ac.be).

D. Fuentes, C. Aramburu, and M. López-Amo are with the Electric and Electronic Department, Public University of Navarre, 31006 Iruña (Pamplona), Nafarroa, Spain.

Digital Object Identifier 10.1109/JSTQE.2002.806679

so that its guided mode is adiabatically transformed into the fundamental mode of the underlying fiber-matched ARROW waveguide. The quasi-guided ARROW modes exhibit very attractive features for a fiber (or silica waveguide) coupling function: large mode sizes, low losses for the fundamental mode, and low polarization and wavelength dependence. Moreover, ARROW waveguides are easy to fabricate owing to their high tolerances and to the fact that the thick core consists of InP. We have also reported work on variants of this structure both in terms of theoretical predictions [12], as well as preliminary experimental results [13].

In this paper, we present a structured overview of the performance of ARROW waveguide-based tapers, whereby we present new results and a better understanding of the potential of this new technique. Section II of this paper presents the theory, design and new results on mode-expanded lasers using fiber-matched vertical ARROW waveguides. Section III demonstrates new relaxed ARROW structures that reduce the overall layer stack thickness significantly without affecting the fiber coupling characteristics. In Section IV, the ARROW effect is used for both vertical and lateral confinement of the output fiber-matched mode, leading to a fabrication scheme for the mode-expanded laser that does not require extra processing steps to integrate the taper. Also, two interesting variants of this concept are proposed and analyzed by simulation. Section V finally summarizes and concludes this work.

II. Mode-Expanded Lasers Using Vertical Arrow Confinement

A. Device Design and Theory

The transverse structure of the proposed mode-expanded laser is shown in Fig. 1. The device consists of an active multiquantum-well (MQW) rib waveguide that is laterally tapered from 3 to 0.3 μm and that contains five 1% compressively strained 80-Å-thick $In_{0.78}Ga_{0.22}As_{0.79}P_{0.21}$ wells for emission at 1.55 μm and four lattice-matched 150-Å-thick $In_{0.75}Ga_{0.25}As_{0.54}P_{0.46}$ barriers, surrounded by 400-Å-thick undoped confining layers having the same composition as the barriers. The metallization covers the SSCs over their entire length in order to avoid absorption losses in the passive section of the taper. This means that there is current injection in a region where low optical gain is provided, increasing the threshold current and reducing the efficiency of these demonstration devices. The optimum metallization stop point should be a compromise between internal absorption loss and threshold current.

The underlying rib waveguide is optimized for coupling to an optical fiber, while keeping in mind the growth-imposed restriction of a maximum overall layer stack thickness of 11 μm. The vertical confinement of this fiber-matched mode is achieved by means of an ARROW geometry that is sketched in more detail in Fig. 2. It consists of an InP core layer with refractive index n_1 and an interference cladding system, i.e., two higher index cladding layers made of quaternary material and a separating InP film, called the second cladding layer. This structure supports a certain number of bound modes in the high index claddings and several leaky waves, which are simply higher

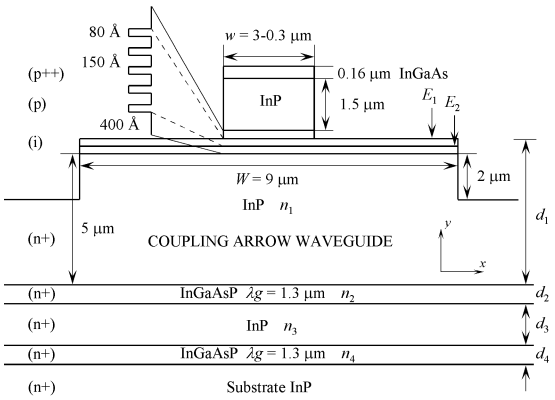

Fig. 1. Schematic drawing of the adiabatic mode-expanded laser showing the tapered upper active rib and the underlying fiber-matched ARROW waveguide.

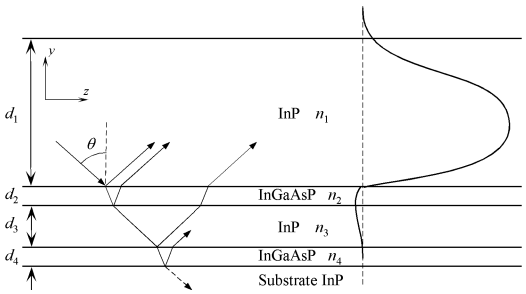

Fig. 2. Core of an ARROW waveguide, bounded at the upper surface by a low-index medium and at the substrate side by two higher index antiresonant reflector layers.

order modes beyond cutoff. Under appropriate conditions, these leaky waves can be confined in the lower index core layer and propagate with relatively low losses. Considering the ray model we can treat it as a case where light coupled into the core undergoes total internal reflection at the upper surface and very high reflections from the sequence of antiresonant Fabry–Pérot resonators formed by the InP–InGaAsP interfaces.

The antiresonance condition for the thickness of the respective cladding layers have been found as [14]

$$d_{2,4} = \frac{\lambda}{4n_{2,4}}\left(1-\left(\frac{n_1}{n_{2,4}}\right)^2+\left(\frac{\lambda}{2n_{2,4}d_{ce}}\right)^2\right)^{-1/2}\cdot(2M+1)$$

$$d_3 = \frac{d_{ce}}{2}(2N+1) \quad (M,N=0,1,2,\ldots) \tag{1}$$

where λ is the vacuum wavelength, n_1, n_2, and n_4 are the refractive index of the ARROW InP core and the first and third cladding layers, respectively, and d_{ce} is the equivalent core thickness, which involves the Goos–Hänchen shift at the top of the ARROW core and is defined as

$$d_{ce} = d_1 + \zeta\frac{\lambda}{2\pi\sqrt{n_{co}^2-n_0^2}} \tag{2}$$

where

$$\zeta = \begin{cases} 1, & \text{for TE modes} \\ \left(\frac{n_0}{n_{co}}\right)^2, & \text{for TM modes.} \end{cases} \tag{3}$$

In the above expressions n_{co} denotes the refractive index of the active core and n_0 the refractive index of the polyimide that

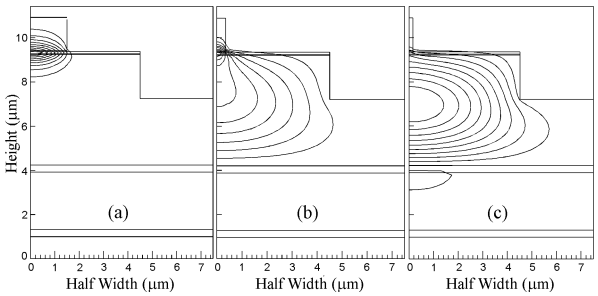

Fig. 3. Fundamental TE mode evolution along the taper structure of Fig. 1 for (a) $w = 3$ μm, (b) $w = 0.7$ μm, and (c) $w = 0.3$ μm. A shallow etch is simulated.

covers the device. We choose a quaternary compound with a bandgap wavelength $\lambda_g = 1.3$ μm for the two high-refractive-index ARROW layers. The thickness of the ARROW core was limited to 5 μm to avoid problems with the growth of a thick layer stack. The calculated thickness of the corresponding cladding layers are $d_{2,4} = 0.32$ μm and $d_3 = 2.6$ μm (TE polarization).

The evolution of the optical field as a function of the upper rib is shown in Fig. 3. As the active waveguide is tapered by reducing the ridge width from 3 to about 0.3 μm, the mode shifts adiabatically from the upper guide to the underlying ARROW waveguide (see Fig. 3).

The design of the lateral taper is based on the adiabaticity of the mode transformation and has been evaluated by means of a commercial three-dimensional (3-D) eigenmode expansion algorithm based on a resonance method [15]. Small taper angles must be kept for the critical widths at which the mode transformation takes place to ensure an adiabatic mode transformation, while large taper angles are allowed for widths where the mode does not significantly change. Two designs, with a different etch depth for the laser rib, have been calculated. The two etch-stop points are indicated as E_1 and E_2 in Fig. 1. The shallow etching E_1 stops just above the layer containing the first quantum well (QW), while the deep etch E_2 goes through the QWs. It is expected that the former option will provide a better performance of the laser because it presents lower surface recombination. On the other hand, when the mode is expanded in the taper, it will be slightly confined in unpumped active quaternary layers [see Fig. 3(c)]. This fact will introduce some absorption losses in the shallowly etched devices that are not present in the deeply etched ones. The adiabatic shape designs for both etching options have been approximated by a piecewise linear device consisting of three linear sections and are sketched in Fig. 4. A minimum narrowing of 100 nm per 66 μm of propagation length yields a safe design from the fabrication point of view.

B. Device Processing

The epitaxial layers were grown by metal–organic chemical vapor deposition (MOCVD). By plasma etching we defined the SiO_x pattern with conventional photoresist as a mask. The central and lateral ribs were etched by RIE to a depth 100 nm above the active layer. Next, a selective wet etch of the remaining InP down to the confining layer of the active layer was carried out. This etch was done using H_3PO_4 : HCl (7:3). Finally, an extra 40 nm (shallow etch) or 140 nm (deep etch) RIE etch into the active layer was performed. Subsequently, a 9-μm-wide and 2-μm-high mesa was wet etched, using the above-mentioned chemistry and parameters, to provide lateral index guiding for the expanded mode. Thereafter, polyimide was spin-coated on the sample to form an insulation layer. The thickness of the polyimide is less on top of the ridges compared to the rest of the sample. Therefore, by a controlled plasma etch, the dielectric was removed on the ridge while dielectric coverage remained elsewhere resulting in good electric isolation [8]. SEM pictures of the taper (Fig. 5) reveal that the metal contact over this upper ridge is good and that the thin ribs were fabricated reproducibly. Next, using a negative photoresist and a metal liftoff process, the metallization pattern was defined. Finally, the thinning of the substrate was done and the back contact was deposited. Arrays of devices, each with 520-μm–long straight active sections, were mounted on electrically cooled copper heatsinks with silver epoxy and were tested without any coatings. The entire device is electrically pumped because the

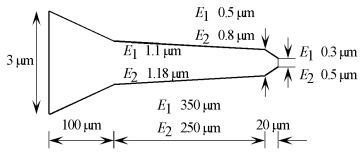

Fig. 4. The optimum taper shape is approximated by a piecewise linear device consisting of three linear sections. Tapers for both shallowly (E_1) and deeply (E_2) etched lasers are shown.

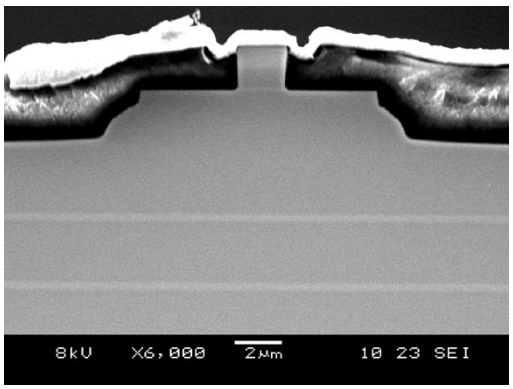

(a)

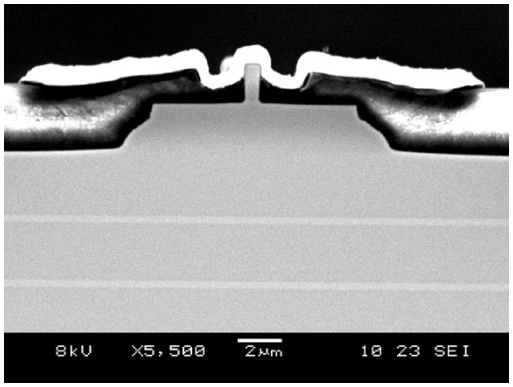

(b)

Fig. 5. SEM image of the laser cross section (a) at the beginning and (b) at the end of the tapering, showing the electric contact over the upper tapered rib and the high-index ARROW cladding layers.

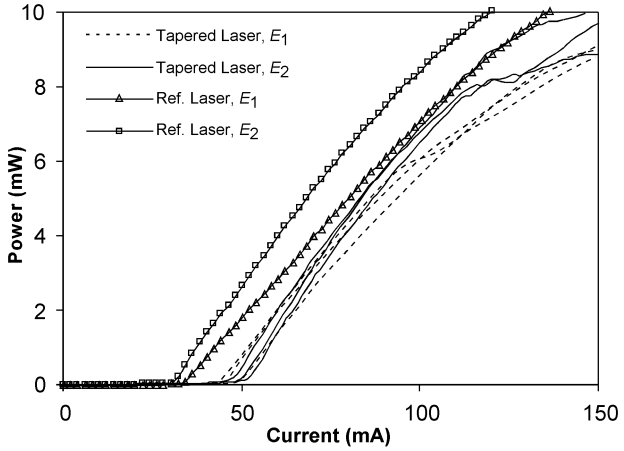

Fig. 6. Typical L–I characteristics of shallowly (E_1) and deeply (E_2) etched mode-expanded and untapered reference lasers.

metallization also covers the entire length of the SSCs. Untapered lasers, 750 μm long and 3 μm wide, fabricated from the same wafer as the tapered lasers, were also prepared as a reference. Both reference and tapered lasers have the same total active area.

C. Results and Discussion

All the measured parameters are shown in Table I for comparison. The devices were operated in CW operation. Some typical room-temperature light intensity versus current ($L-I$) curves of mode-expanded and untapered reference lasers are shown in Fig. 6 for both etch depths. The deeply etched reference devices, with a threshold current of 30 mA and an external efficiency of 0.13 W/A, present a slightly better laser performance than the shallowly etched ones, which have a similar threshold current but a lower external efficiency (0.09 W/A). The deeply etched devices always show a better performance as we will see in the next sections of this paper. Fairly uniform threshold current distributions were found along the laser array.

Regarding the mode-expanded lasers, an increase of about 20 mA in the threshold current with respect to the reference lasers is found. This is a common behavior due to the mode transformation loss within the taper and to the losses in the n-doped thick InP ARROW core layer and not to the introduction of the ARROW. A shorter current pumping length would reduce the threshold current. A higher slope efficiency is observed for the expanded mode laser. This surprising result can be attributed to a difference in reflectivity between the laser mode and the expanded mode [16], which can account for about 15% difference in output power. For the shallowly etched devices, however, the mentioned increase is not so prominent since the efficiency is adversely influenced by the higher absorption loss in the unpumped QWs next to the central laser ridge [see Fig. 3(c)].

Far-field emission patterns for both tapered and reference lasers were measured by using a rotating stage and a pinhole detector. The measured full-width at half-maximum (FWHM) values are also shown in Table I, which are in good agreement with theoretical calculations obtained from the Fourier transform of the theoretical near fields. An important lateral divergence improvement is achieved for both groups of lasers, reaching a minimum of 10° for the deeply etched lasers. This value should be compared with the 30° divergence of the reference devices. The vertical farfield is determined by the thickness of the ARROW slab core, which is limited by the maximum layer stack thickness as mentioned before. The achieved vertical field divergences are therefore higher (22° and 27° for both sets of lasers respectively, see Table I), but are still substantially lower than the 40° of the reference devices.

A coupling efficiency measurement was performed between the expanded mode laser and a standard cleaved single-mode fiber with a spot size of 10 μm at 1.55 μm. Fiber coupling efficiencies better than -3 dB are obtained for both etch depths, including the Fresnel losses occurring at the air–glass interface. The improvement in the fiber coupling with respect to the untapered devices amounts up to 5.4 dB for the deeply etched lasers (see Table I).

Since the alignment tolerance with respect to the fiber depends on the large fiber mode, only slight improvements are observed with respect to the reference untapered lasers. A maximum -1 dB alignment tolerance of $\pm 2.2 \times \pm 2.3$ μm (lateral $\times$ vertical) is obtained for the deeply etched devices. The fact that the vertical alignment tolerance is higher than the lateral value is due to the fact that the fiber facet was separated from the taper output facet. These restrictions were considered to avoid contact of the fiber end with the laser output facet during the sweep of the transverse position of the fiber.

All results reported in Table I are in good agreement with theoretical calculations.

III. New Vertical ARROW Structures for Mode-Expanded Lasers

A. Design

The three vertical ARROW cladding layers (d_2, d_3, and d_4) used in the device of Section II are designed to generate an antiresonance condition and provide minimum leakage loss toward the substrate for the fiber-matched output waveguide. However, from (1) and (2), it can be seen that the total thickness of this optimum cladding is higher than half the InP ARROW core thickness, which can be considered to be rather thick. Since the expanded ARROW-confined output mode is only guided over a short distance, it is not really necessary to reduce the ARROW losses to an absolute minimum. In other words, it is allowed to move away from the antiresonance condition, thus increasing the radiation but also reducing the thickness of the cladding layers [12]. Fig. 7 shows the leakage loss for the 5-μm-thick ARROW waveguide used in the device of Section II and calculated using the transfer matrix method (TMM) [17]. The leakage loss for the optimum design is 0.25 dB/cm. If a maximum propagation length of 300 μm is considered for the ARROW mode in the taper and a reasonable total leakage loss of 0.1 dB is allowed, the new claddings may exhibit a leakage loss as high as 3 dB/cm. The line that keeps this criterion is highlighted in Fig. 7. The relaxed structure with a leakage loss of 3 dB/cm is $d_{2,4} = 0.31$ μm and $d_3 = 0.5$ μm, reducing the total cladding thickness to 1.12 μm, which is 2.12 μm less than the optimum structure.

TABLE I
MEASUREMENT AND SIMULATION RESULTS ON THE INTEGRATED MODE-EXPANDED LASERS CONSIDERED IN THIS WORK: $I_{\rm th}$ = THRESHOLD CURRENT; η_d = EXTERNAL EFFICIENCY; L = TAPER LENGTH; FC = FIBER-COUPLING EFFICIENCY; FF = FAR-FIELD DIVERGENCE ANGLES; $Tol.$ = -1 dB ALIGNMENT TOLERANCE. THE LAST TWO ROWS CORRESPOND TO SIMULATION RESULTS

Taper	Laser	Etching Depth	I_{th} (mA)	η_d (W/A)	L (μm)	FC (dB)	FF		$Tol.$ (±)	
							L (Deg.)	V (Deg.)	L (μm)	V (μm)
Vertical ARROW	Reference	E_1	31	0.09	0	–8.2	30.5	43	1.9	2.1
		E_2	30	0.13	0	–8	30.1	40.1	1.5	2
	Tapered	E_1	45	0.1	470	–2.9	10.4	22	2	2.2
		E_2	50	0.15	370	–2.6	10	27	2.2	2.3
Relaxed Vertical ARROW	Reference	E_1	35	0.13	0	–8	30.3	39	1.8	2.1
		E_2	22	0.13	0	–8.2	30.9	40.7	2	2.3
	Tapered	E_1	60	0.11	470	–2.7	11	19	2.3	2.4
		E_2	32	0.1	370	–2.9	9.6	25	2.4	2.5
Lateral ARROW	Reference	E_1	35	0.12	0	–8	31.5	42.8	1.6	2
		E_2	28	0.12	0	–8.3	30.7	40.6	1.5	2
	Tapered	E_1	55	0.1	520	–4	13.8	30.8	2.3	2.4
		E_2	48	0.12	490	–4.3	13	32.7	2.2	2.3
Variant 1, Fig. 16		E_2	–	–	490	–2.4	7.2	14	2.3	1.9
Variant 2, Fig. 17		Buried	–	–	270	–1.1	7.2	9	2.9	2.3

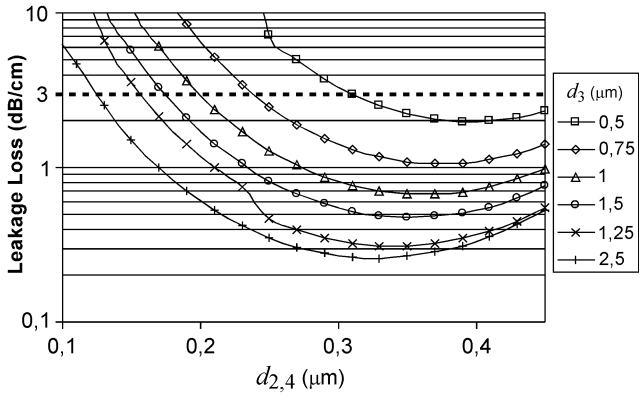

Fig. 7. Attenuation of the fundamental TE ARROW mode as a function of the thickness of the three cladding layers d_2, d_3, and d_4 for a core thickness $d_1 = 5$ μm.

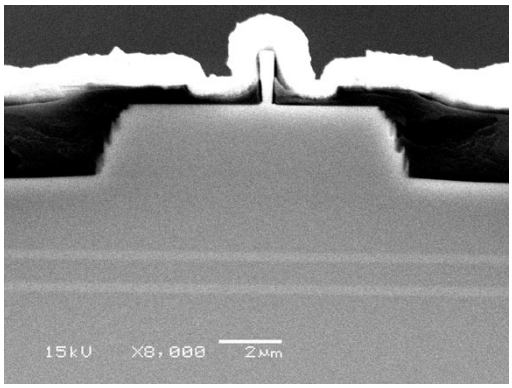

Fig. 8. SEM image of the laser cross section using the relaxed ARROW structure.

Both shallowly and deeply etched devices were again implemented on a new wafer incorporating the new relaxed vertical ARROW structure and using the same processing as explained in Section II. Fig. 8 shows the SEM photograph of one device. The operation of the mode expanders is not influenced by substituting the ARROW cladding structure with the relaxed design and the adiabatic taper shapes calculated in Section II and shown in Fig. 4 are still valid here. New arrays of devices, each with 520 μm long straight active sections were mounted. Untapered lasers, 750 μm long and 3 μm wide and fabricated from the same wafer as the tapered lasers, were also prepared as a reference.

B. Results

The CW room-temperature $L-I$ curves of several mode-expanded and untapered reference lasers are shown in Fig. 9 for both etch depths. The measured parameters are summarized in Table I. The deeply etched untapered lasers present the best performance. They show a threshold current around 22 mA, while the shallowly etched lasers exhibit a threshold of 35 mA.

Regarding the mode-expanded lasers, an increase of only 10 mA in the threshold current with respect to the reference is found for the deeply etched devices. In the case of the shallowly etched devices, this increase in the threshold is of 25 mA.

The coupling efficiency to a standard single-mode fiber does not change and also the lateral FWHM divergence angles remain

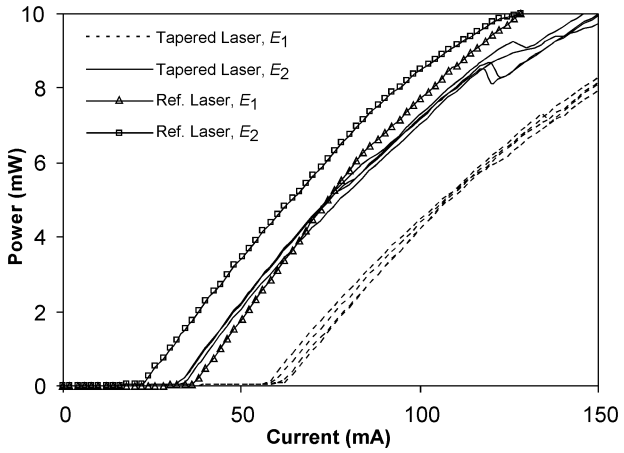

Fig. 9. Typical L–I characteristics of shallowly (E_1) and deeply (E_2) etched untapered reference lasers and mode-expanded lasers incorporating the relaxed ARROW structure.

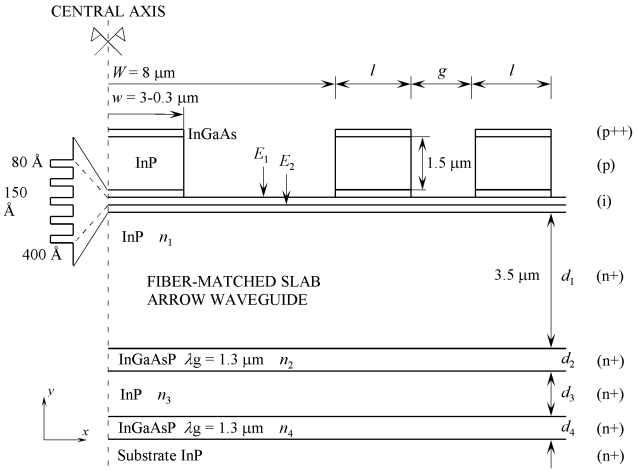

Fig. 10. Cross section of the device that uses the antiresonant effect for both the lateral and the vertical confinement.

the same. The vertical divergence angles, however, are reduced by a few degrees, as predicted by theoretical calculation [12]. The reason for this slight improvement is the reduction of the light in the new relaxed d_2, d_3, and d_4 cladding layers. The sign of the optical field in these layers [see Fig. 3(c)] is opposed to the sign of the field in the InP core [14] and reduces the fiber coupling efficiency and the far-field divergence angles.

A maximum -1 dB alignment tolerance of around $\pm 2.4 \times \pm 2.5$ μm (lateral $\times$ vertical) is obtained for both sets of devices.

IV. Mode-Expanded Lasers Using Vertical and Lateral Arrow Confinement

A. Device Design and Theory

The antiresonant effect can be used, not only for the vertical confinement, but also for the lateral confinement of the output fiber-matched mode [13], [18], [19]. The objective of this new device is to drastically simplify the fabrication process by eliminating the second etch step in which the broad underlying waveguide is defined. This eliminates the alignment of the second mask and reduces the fabrication complexity of the mode-expanded laser to that of a standard laser.

Fig. 10 shows the right half of the cross section of the proposed device. The laser structure and lower ARROW cladding materials are the same as in the previous devices. The lower InP core thickness is reduced to 3.5 μm because the lateral ribs lose their influence on the optical confinement when thicker layers are used. If thicker cores were needed, then more than two lateral ribs would have to be used. From (1)–(3), the optimum ARROW cladding is found to be $d_{2,4} = 0.32$ μm and $d_3 = 1.86$ μm. Relaxed structures to reduce the layer stack thickness could be found in a similar way as discussed in Section III [12].

A couple of appropriately designed rib waveguides placed on each side of the tapered central waveguide and defined in the same etch step as the central laser ridge provide the lateral confinement of the guided mode. The behavior cannot be explained with the standard vertical ARROW formulas because of the guided modes that appear in the lateral ribs. Considering two-dimensional (2-D) coupled-mode theory, the new mode can be treated intuitively as an anti-symmetrical combination of the

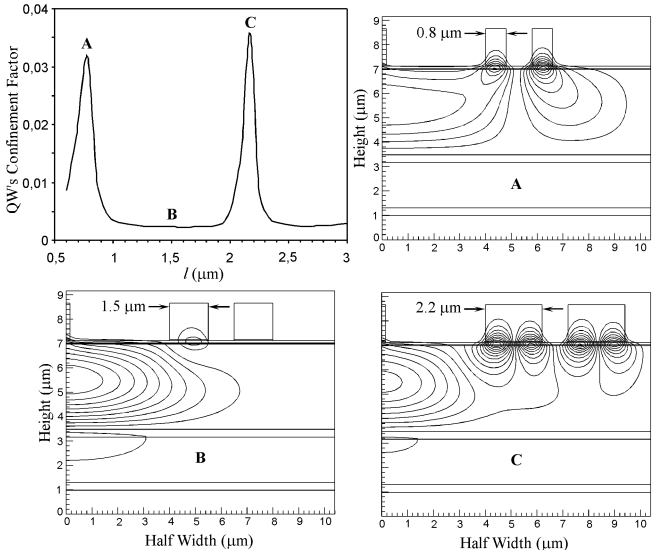

Fig. 11. Confinement of the output mode in the unpumped QWs in the lateral ARROW ribs of a shallowly etched device as a function of the width l of the lateral ribs keeping the gap g constant. The field distributions of the modes at the points indicated in the graph are also shown.

coupled modes of the upper lateral rib waveguides and the mode of the underlying InP slab ARROW core [20]. Thus, the shape of the output mode depends strongly on the width of the lateral ribs. Fig. 11 shows the confinement of the fiber-matched leaky mode in the unpumped QWs of the lateral ribs as a function of the lateral rib width l while keeping the gap g constant and equal to 1 μm. This confinement should be minimized in order to reduce absorption loss in the unpumped lateral ribs. The field profiles for different widths l are also shown for illustration. A flat and broad minimum confinement is found around $l = 1.5$ μm, where the output mode is fit for coupling to fiber. The broad minimum implies that the device is tolerant to fabrication errors. Two designs, with a different etch depth for the central laser rib, are considered once again (shown as E_1 and E_2 in Fig. 10) and the optimum width l for the deeply etched device is also calculated and found to be 1.6 μm. In both etch options the optimum gap g between lateral ribs is less than

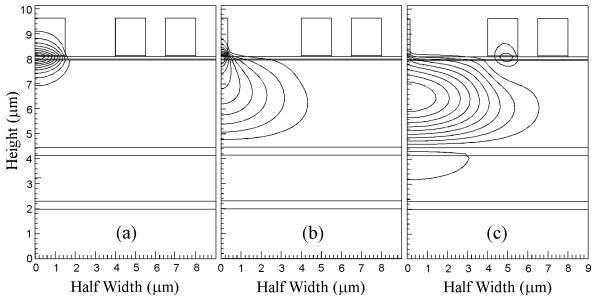

Fig. 12. Fundamental TE mode evolution along the taper structure of Fig. 10 for (a) $w = 3$ μm, (b) $w = 0.7$ μm, and (c) $w = 0.3$ μm (shallow etch).

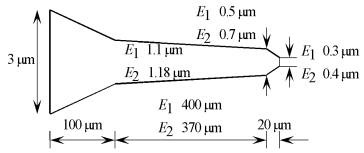

Fig. 13. Piecewise linear approximation of the ideal taper shape for the device with both vertical and lateral ARROW confinement. Tapers for both a shallowly (E_1) and deeply (E_2) etched laser are shown.

1 μm, but has to be increased to 1 μm because of fabrication limitations. Fortunately, this does not change the modal shape significantly.

The evolution of the optical field as a function of the upper central rib width is shown in Fig. 12. As the active waveguide is tapered by reducing the ridge width from 3 to 0.3 μm, the mode shifts adiabatically from the upper guide to the underlying ARROW waveguide (Fig. 12). The design of the lateral tapering is based on the adiabaticity of the mode transformation and has been evaluated by means of a commercial 3-D eigenmode expansion. The adiabatic shape designs for both etching options have been approximated by a piecewise linear device consisting of three linear sections and are sketched in Fig. 13. A minimum narrowing of 100 nm per 77 μm propagation length yields a safe design from the fabrication point of view.

The expanded mode in the shallowly etched device is slightly confined in unpumped active quaternary layers [see Fig. 12(c)]. This will introduce some absorption losses in the shallowly etched lasers that are not present in the deeply etched designs.

B. Device Processing

A wafer with the new layer structure was grown by MOCVD and the devices were implemented using the same processing steps as detailed in Section II (except, of course, the wet etching of the broad rib). Fig. 14 shows an SEM picture of the device, illustrating the contacting of the central ridge and the well-defined lateral ribs. Once again, arrays of devices, each with 520-μm-long straight active sections, were mounted on electrically cooled copper heatsinks with silver epoxy and were tested without any coatings. Untapered lasers (750 μm$\times 3$ μm) fabricated from the same wafer as the tapered lasers were also prepared as a reference.

C. Results and Discussion

All the measured parameters are shown in Table I. Typical room-temperature L–I curves of mode-expanded and untapered reference lasers are shown in Fig. 15 for both etch depths. The

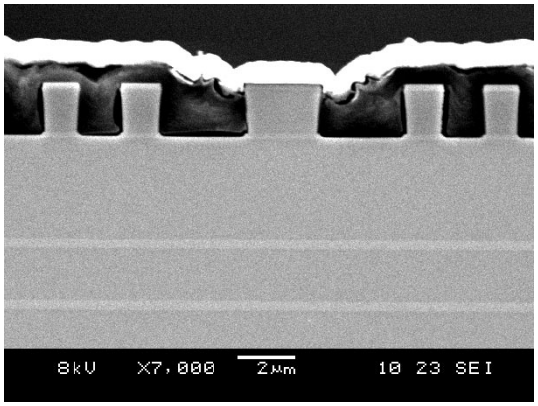

Fig. 14. SEM image of the laser cross section, showing the electric contact over the central tapered rib, the good definition of the lateral ribs, and the high-index ARROW cladding layers.

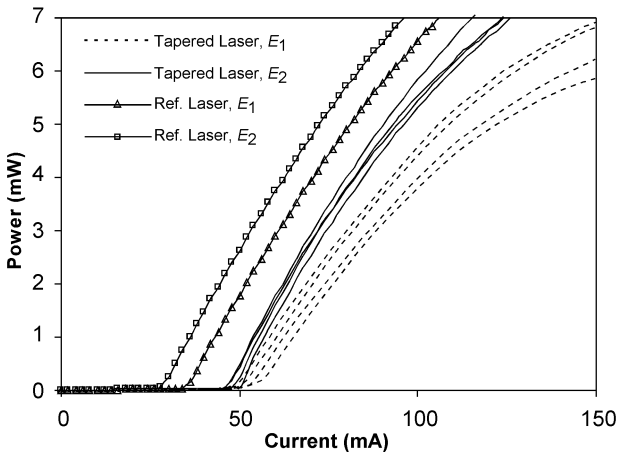

Fig. 15. Typical L–I characteristics of shallowly (E_1) and deeply (E_2) etched untapered reference lasers and mode-expanded lasers using the vertical and lateral ARROW-confined fiber-matched waveguide.

deeply etched reference devices, with a threshold current of 28 mA, present a better laser performance than the shallowly etched ones (35 mA). A uniform threshold current distribution was found along the laser array once again.

Regarding the mode-expanded lasers, an increase of about 20 mA in the threshold current with respect to the reference lasers is found. The higher absorption loss in the unpumped QWs of the lateral ARROW rib waveguides for the shallowly etched devices [see Fig. 12(c)] causes a decrease of the external efficiency of the laser from 0.12 to 0.1 W/A. This fact is not observed in the deeply etched devices that maintain the same external efficiency as the reference lasers.

The measured FWHM values are also shown in Table I. A considerable improvement is achieved in the lateral direction for both groups of lasers, reaching a minimum of 13° for the deeply etched lasers. On the other hand, due to the thinner ARROW slab core (3.5 μm), the achieved vertical field divergence is still slightly higher than 30°, improving it by 10° with respect to the reference laser. A further improvement in the vertical far-field pattern could be obtained by thickening the ARROW core layer and defining more than two ribs on each side of the output ARROW waveguide in order to provide a good lateral confinement for thick cores.

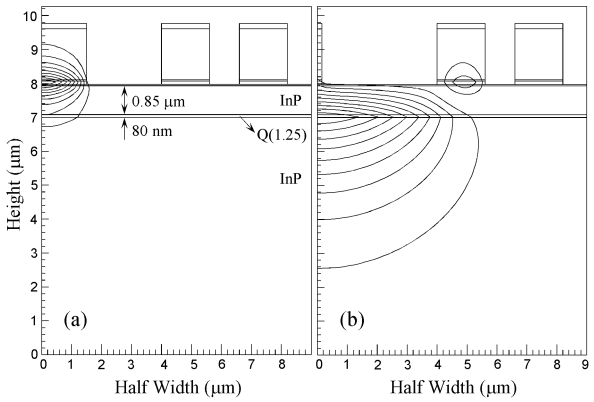

Fig. 16. Schematic structure of the taper using a weakly guiding underlying slab waveguide. The active layer and upper rib waveguides are identical to those of Fig. 10.

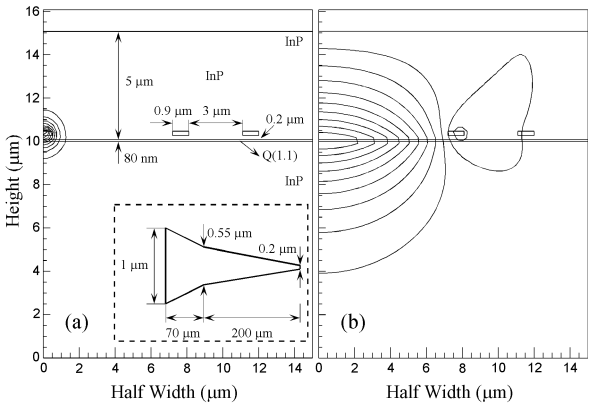

Fig. 17. Schematic structure of a buried variant of the proposed taper concept.

Maximum fiber coupling efficiencies of around -4 dB are obtained for both etch depths, including the Fresnel losses occurring at the air–glass interface. The improvement in the fiber coupling with respect to the untapered devices amounts up to 4 dB (see Table I). A maximum -1 dB alignment tolerance of around $\pm 2.3 \times \pm 2.4$ μm is obtained for both sets of lasers.

Again, all the results are in good agreement with theoretical calculations.

D. Variant 1: Weakly Guiding Fiber-Adapted Waveguide

The waveguide structure of Fig. 10 has a limitation on the vertical direction because the lateral ribs lose their optical confinement effect when the slab core becomes too thick. The structure of Fig. 16 is similar to that of Fig. 10 but it makes use of a thin weakly guiding core of only 80 nm that is buried in InP beneath the active layer. The mode at the active rib and the mode at the end of the taper are also shown. The fiber-matched mode presents a quite asymmetrical field distribution in the vertical direction, but the fact that its maximum is closer to the upper lateral couple of ribs strengthens their influence. Moreover, from a coupling and far-field point of view the typical exponential decay of weakly guiding waveguides induces an improvement of the coupling efficiency and FWHM of the output beam in comparison with the untapered lasers, in spite of its asymmetrical shape.

Simulation results on the propagation of this new structure are shown in Table I. Only the design for the deep etching through the QWs has been considered because of its better lasing performance. The same tapering as sketched in Fig. 13 has been simulated. It appears that the beam divergence angles and the coupling efficiency are improved to $7.2^\circ \times 14^\circ$ (lateral $\times$ vertical) and -2.4 dB, respectively. The vertical alignment tolerance is slightly reduced to ± 1.9 μm, while the lateral value remains the same as for the vertical ARROW design.

E. Variant 2: Buried Laser

The mode transformation concept proposed in this section can also be integrated in a second variant, being a buried laser structure as shown in Fig. 17. A 194-nm-thick buried MQW active structure with an equivalent refractive index of 3.45 is tapered from 1 to 0.2 μm following the tapering shown in the inset of Fig. 17(a). The 70-nm thin guiding layer of quaternary compound with $\lambda_g = 1.1$ μm is buried 0.2 μm beneath the active core. The optimum lateral confinement ARROW ribs are 0.9 μm wide and are separated by 2 μm. All this is embedded under a 5-μm-thick top layer of InP.

The fact that the tapered active central core is totally embedded in InP makes the mode transformation efficiency much higher for buried than for rib structures. This is the reason why the length of the buried taper (270 μm) is much shorter than the rib taper (490 μm).

Simulation results on the propagation are shown in Table I. They show fiber butt coupling losses as low as 1.1 dB, beam divergence angles of $7.2^\circ \times 9^\circ$ (lateral $\times$ vertical) and alignment tolerances of $\pm 2.9 \times \pm 2.3$ μm (lateral $\times$ vertical), compared to the 8.5-dB coupling loss and $29^\circ \times 32^\circ$ divergence angles of the untapered devices.

V. Conclusion

In this paper, we have presented the use of optical confinement by the ARROW concept for the fabrication of lasers with monolithically integrated SSCs. This eliminates the need for thick $In_{1-x}Ga_xAs_yP_{1-y}$ layers and the consequential growth problems. The taper transforms the small active laser mode into the fiber-adapted mode of the large underlying mesa with vertical ARROW confinement. Threshold currents of around 50 mA were measured, which have to be compared with 30 mA for untapered reference lasers. The far-field FWHM divergence angles were significantly reduced and the coupling efficiency to single-mode fiber was improved by 5.4 dB.

We also calculated that the ARROW cladding thickness can be reduced drastically by moving away from the optimal antiresonance condition without introducing remarkable extra losses. The new structures significantly reduce the overall layer stack thickness while maintaining the far-field divergence angles and the fiber coupling efficiency of the optimum ARROW structures.

Lateral ARROW confinement, in combination with vertical confinement, was also successfully demonstrated. The lateral confinement of the fiber-matched mode is achieved by means of an antiresonant effect provided by two sets of lateral rib waveguides defined in the same etching process as the central active ridge. Therefore, only a single planar growth step and a single

conventional etching process are required, leading to the simplest tapered laser concept ever reported. Threshold currents of around 50 mA were measured, which have to be compared with 30 mA for untapered lasers. The far-field FWHM divergence angles were significantly reduced and a 4-dB improvement of the coupling efficiency to single mode fiber was observed.

Two variants of the demonstrated concept have also been analyzed by simulation and are expected to show a better performance. In a first variant, a weakly guiding slab waveguide substitutes the thicker core of the first structure. In a second variant, the taper concept of this work is integrated in a buried laser structure. Simulation results show considerable improvements in the far-field divergence angles and fiber-coupling efficiencies.

REFERENCES

[1] I. Moerman, P. Van Daele, and P. M. Demeester, "A review on fabrication technologies for the monolithic integration of tapers with III–V semiconductor devices," *IEEE J. Select. Topics Quantum Electron.*, vol. 3, pp. 1308–1320, Dec. 1997.

[2] T. Alder, A. Stöhr, R. Heinzelmann, and D. Jäger, "High-efficiency fiber-to-chip coupling using low-loss tapered single-mode fiber," *IEEE Photon. Technol. Lett.*, vol. 12, pp. 1016–1018, Aug. 2000.

[3] Y. Suzaki, K. Magari, Y. Kondo, Y. Kawaguchi, Y. Kadota, and K. Yoshino, "High-gain array of semiconductor optical amplifier integrated with bent spot-size converter (BEND SS-SOA)," *J. Lightwave Technol.*, vol. 19, pp. 1745–1750, Nov. 2001.

[4] D. Jang, J. Shim, J. Lee, and Y. Eo, "Asymmetric output characteristics in 1.3-μm spot-size converted laser diodes," *IEEE J. Quantum Electron.*, vol. 37, pp. 1611–1617, Dec. 2001.

[5] S. S. Saini, F. G. Johnson, D. R. Stone, H. Shen, W. Zhou, and M. Dagenais, "Passive active resonant coupler (PARC) platform with mode expander," *IEEE Photon. Technol. Lett.*, vol. 12, pp. 1025–1027, Aug. 2000.

[6] G. A. Vawter, A. T. Sullivan, J. R. Wendt, R. E. Smith, H. Q. Hou, and J. F. Klem, "Tapered rib adiabatic following fiber couplers in etched GaAs materials for monolithic spot-size transformation," *IEEE J. Select. Topics Quantum Electron.*, vol. 3, pp. 1361–1371, Dec. 1997.

[7] K. De Mesel, R. Baets, C. Sys, S. Verstuyft, I. Moerman, and P. Van Daele, "First demonstration of a 980 nm oxide confined laser with integrated spot size converter," *Electron. Lett.*, vol. 36, pp. 1028–1029, June 2000.

[8] V. Vusirikala, S. S. Saini, R. E. Bartolo, S. Agarwala, R. D. Whaley, F. G. Johnson, D. R. Stone, and M. Dagenais, "1.55-μm InGaAsP–InP laser arrays with integrated-mode expanders fabricated using a single epitaxial growth," *IEEE J. Select. Topics Quantum Electron.*, vol. 3, pp. 1332–1343, Dec. 1997.

[9] M. Galarza, K. De Mesel, S. Verstuyft, C. Aramburu, I. Moerman, P. Van Daele, R. Baets, and M. Lopez-Amo, "1.55 μm InP–InGaAsP Fabry–Pérot lasers with integrated spot size converters using antiresonant reflecting optical waveguides," *IEEE Photon. Technol. Lett.*, vol. 14, pp. 1043–1045, Aug. 2002.

[10] M. A. Duguay, Y. Kokubun, T. L. Koch, and L. Pfeiffer, "Antiresonant reflecting optical waveguides in SiO_2-Si multilayer structures," *Appl. Phys. Lett.*, vol. 49, no. 1, pp. 13–15, July 1986.

[11] T. L. Koch, U. Koren, G. D. Boyd, P. J. Corvini, and M. A. Duguay, "Antiresonant reflecting optical waveguides for III–V integrated optics," *Electron. Lett.*, vol. 23, pp. 244–245, Feb. 1987.

[12] M. Galarza, K. De Mesel, D. Fuentes, R. Baets, and M. Lopez-Amo, "Modeling of InGaAsP–InP 1.55 μm lasers with integrated mode expanders using fiber matched leaky waveguides," *Appl. Phys. B*, vol. 73, pp. 585–588, Oct. 2001.

[13] M. Galarza, K. De Mesel, T. Van Caenegem, S. Verstuyft, C. Aramburu, I. Moerman, P. Van Daele, R. Baets, and M. López-Amo, "InGaAsP–InP 1.55 μm lasers with integrated mode expanders using fiber-matched leaky waveguides," in *Proc. LEOS '01 Annu. Meeting*, San Diego, CA, November 2001, pp. 798–799.

[14] J. M. Kubica, "Numerical analysis of InP/InGaAsP ARROW waveguides using transfer matrix approach," *J. Lightwave Technol.*, vol. 10, pp. 767–771, June 1992.

[15] A. S. Sudbo, "Numerically stable formulation of the transverse resonance method for mode-field calculations in dielectric waveguides," *IEEE Photon. Technol. Lett.*, vol. 5, pp. 342–344, Mar. 1993.

[16] M. Reed, T. M. Benson, P. C. Kendall, and P. Sewell, "Antireflection coated angled facet design," *Proc. Inst. Elect. Eng.*, pt. J, pp. 214–220, 1996.

[17] J. Chilwell and I. Hodgkinson, "Thin-films field-transfer matrix theory of planar multilayer waveguides and reflection from prism-loaded waveguides," *J. Opt. Soc. Amer. B*, vol. 1, pp. 742–753, July 1984.

[18] L. J. Mawst, D. Botez, C. Zmudzinski, and C. Tu, "Design optimization of ARROW-type diode lasers," *IEEE Photon. Technol. Lett.*, vol. 4, pp. 1204–1206, Nov. 1992.

[19] ——, "Antiresonant reflecting optical waveguide-type, single-mode diode laser," *Appl. Phys. Lett.*, vol. 61, no. 5, pp. 503–505, Aug. 1992.

[20] G. R. Hadley, "Two-dimensional coupled-mode theory for modeling leaky-mode arrays," *Opt. Lett.*, vol. 15, pp. 27–29, Jan. 1990.

Marko Galarza was born in Urdiain, Spain, in 1973. He received the Ingeniero de Telecommunicación degree from the Public University of Navarra, Pamplona, Spain, in 1997. He is currently working toward the Ph.D. degree in electrical engineering at the University of Ghent, Gent, Belgium.

While at the Public University of Navarra, he worked in the field of integrated optics until 2000.

Kurt De Mesel was born in Poperinge, Belgium, in 1972. He received the degree in electrical engineering from the University of Ghent, Gent, Belgium, in 1997, where he is currently working toward the Ph.D. degree in electrical engineering.

His research interests include modeling, design, and fabrication of spot-size converters and oxide-confined devices.

Steven Verstuyft is responsible for the processing of III–V optoelectronic devices at the Department of Information Technology of the University of Ghent, Gent, Belgium.

David Fuentes was born in Tudela, Spain. He received the Ingeniero de Telecomunicación degree from Public University of Navarra, Pamplona, Spain, in 2001.

Cándido Aramburu was born in San Sebastián, Spain, on July 1964. He received the Ingeniero de Telecommunicación degree from the Universidad Politécnica de Madrid, Madrid, Spain, in 1989 and the Ph.D. degree in telecommunications engineering from the Public University of Navarre, Pamplona, Spain, in 2001.

From 1992 to 1994, he was an Associate in Computers and from 1995 in Electronics and Photonics Devices at the Electrical and Electronical Engineering Department of Public University of Navarre, Pamplona, Spain. Since 1995 he has worked in the field of integrated optics with emphasis in the InGaAsP–InP passive and active devices.

Manuel López-Amo (M'91–SM'98) was born in Madrid, Spain, in June 1960. He received the Ingeniero de Telecomunicación degree and the Ph.D. degree in telecommunications engineering both from the Universidad Politécnica de Madrid, Madrid, Spain, in 1985 and 1989, respectively.

From 1985 to 1989 he was a lecturer in Optical Communications and Electronics at the Photonic Technology Department of the Universidad Politécnica de Madrid. During 1987, he was a visiting Ph.D. student at the Laboratorium Voor Elektromagnetisme en Acustica of the University of Ghent (Belgium), working on Integrated Optics. In January 1990, he became an Associate Professor with the Photonic Technology Department of the Universidad Politécnica de Madrid. From 1990 to 1995 he was teaching Optical Communications for undergraduate and post-graduate students. In 1992, he was a Visiting Researcher at British Telecom Research Labs, Ipswich, U.K., working in amplified fiber-optic networks. In March 1996 he obtained a chair as Full Professor in the Public Univesity of Navarre, Pamplona, Spain, in the Electrical and Electronical Engineering. Now he is the Head of this Department. He has coauthored more than 100 works in journals and conferences all related with fiber-optic networks, fiber optic components, optical amplifiers, fiber-optic processors, fiber-optics sensors, and integrated optics.

Ingrid Moerman (M'96) was born in Gent, Belgium, in 1965. She received the degree in electrical engineering and the Ph.D. degree from Ghent University, Gent, Belgium, in 1987 and 1992, respectively.

Since 1987, she has been with the Interuniversity Micro-Electronics centre (IMEC) at the Department of Information Technology (INTEC) of Ghent University. Her main contributions are the epitaxial growth of III–V optoelectronic components and photonic integrated circuits for telecom applications. In 1997, she became a permanent member of the Research Staff at IMEC, where she coordinates the research on the epitaxial growth of III–V optoelectronic devices. Since 2000, she has been a part-time Professor with Ghent University. She has recently expanded her research domain to broad-band communication networks, more specifically mobile communications. She is the author or coauthor of more than 250 publications in the field of optoelectronic components and technology.

Peter Van Daele received the Ph.D. degree in electrical engineering from the University of Ghent, Gent, Belgium, in 1988.

He then became a permanent member of staff of IMEC, the Department of Information Technology, University of Ghent, where he is responsible for the research on processing of III–V optoelectronic devices. Since 2001 his work has focused more on optical packaging and optical interconnections, with emphasis on coupling to fiber arrays, integration on printed circuit boards, and the use of laser processing techniques. In 1993 he also became part-time Professor. He is the author or coauthor of about 200 publications in the field of optoelectronic components and technology.

Roel G. Baets (M'88–SM'96) received the degree in electrical engineering from Ghent University, Gent, Belgium, in 1980, the M.Sc. degree in electrical engineering from Stanford University, Stanford, CA, in 1981, and the Ph.D. degree from Ghent University in 1984.

Since 1981 he has been with the Department of Information Technology (INTEC) of Ghent University. Since 1989, he has been a Professor on the engineering faculty of Ghent University. From 1990 till 1994, he was also a part-time Professor with the Technical University of Delft, The Netherlands. He has mainly worked in the field of III–V devices for optoelectronic systems. With about 300 publications and conference papers as well as about 10 patents, he has made contributions to the design and fabrication of semiconductor laser diodes, passive guided wave devices, photonic integrated circuits, and microoptic components. He leads the Optoelectronic Components and Systems group at Ghent University–INTEC (which is an associated lab of IMEC), working on photonic devices for optical communication and optical interconnect.

Prof. Baets is a member of the Optical Society of America, the IEEE Lasers and Electro-Optics Society (IEEE-LEOS), SPIE, and the Flemish Engineers Association. He has been a member of the program committees of OFC, ECOC, IEEE Semiconductor Laser Conference, ESSDERC, CLEO-Europe, and the European Conference on Integrated Optics. He was chairman of the IEEE-LEOS Benelux chapter from 1999 to 2001.